ADVANCES IN TIME AND FREQUENCY TRANSFER FROM DUAL-FREQUENCY GPS PSEUDORANGE AND CARRIER-PHASE OBSERVATIONS

François Lahaye, Paul Collins
Geodetic Survey Division, Natural Resources Canada (NRCan)
Ottawa, Canada
Francois.Lahaye@nrcan-rncan.gc.ca
Paul.Collins@nrcan-rncan.gc.ca

Giancarlo Cerretto and Patrizia Tavella
Istituto Nazionale di Ricerca Metrologica (iNRiM)
Torino, Italy
g.cerretto@inrim.it
p.tavella@inrim.it

Abstract

Although carrier-phase observations are thought to drive the accuracy of time and frequency transfer accuracy obtainable using geodetic GPS receivers, there has been evidence of how colored noise on the pseudorange observations reduces the effectiveness of the technique. We present a new parameterization of the GPS pseudorange and carrier-phase observations, called the decoupled-clock model, where a pseudorange bias is estimated for each clock in the system as a white noise parameter. The new parameterization separates the pseudorange observation colored noise from the carrier-phase parameters (ambiguities and clock), and also isolates the ambiguities as integer-valued parameters. While ambiguous, the carrier-phase clock estimates yield continuous frequency estimates at carrier-phase precision over carrier-phase continuous periods. The obtained frequencies are consistent with those implied by the International GNSS Service Rapid clock products without solution-boundary discontinuities. The supporting rationale for the decoupled-clock model is presented from recently published literature and actual processing examples. The carrier-phase clock solutions are compared to the IGS Rapid solutions and common clock parameterization. Combination methods are considered, including the re-introduction of observed pseudoranges through functions of the estimated pseudorange biases, with the goal of bridging losses of lock on the constellations, and removal of the ambiguity in the carrier-phase clocks to yield time transfer capability.

Report Documentation Page

Form Approved
OMB No. 0704-0188

1. REPORT DATE	2. REPORT TYPE	3. DATES COVERED
01 DEC 2008	**N/A**	**-**

4. TITLE AND SUBTITLE	5a. CONTRACT NUMBER
Advances In Time And Frequency Transfer From Dual-Frequency Gps Pseudorange And Carrier-Phase Observations	5b. GRANT NUMBER
	5c. PROGRAM ELEMENT NUMBER
6. AUTHOR(S)	5d. PROJECT NUMBER
	5e. TASK NUMBER
	5f. WORK UNIT NUMBER
7. PERFORMING ORGANIZATION NAME(S) AND ADDRESS(ES) **Geodetic Survey Division, Natural Resources Canada (NRCan) Ottawa, Canada**	8. PERFORMING ORGANIZATION REPORT NUMBER
9. SPONSORING/MONITORING AGENCY NAME(S) AND ADDRESS(ES)	10. SPONSOR/MONITOR'S ACRONYM(S)
	11. SPONSOR/MONITOR'S REPORT NUMBER(S)

12. DISTRIBUTION/AVAILABILITY STATEMENT
Approved for public release, distribution unlimited

13. SUPPLEMENTARY NOTES
See also ADM002186. Annual Precise Time and Time Interval Systems and Applications Meeting (40th) Held in Reston, Virginia on 1-4 December 2008, The original document contains color images.

14. ABSTRACT

15. SUBJECT TERMS

16. SECURITY CLASSIFICATION OF:			17. LIMITATION OF ABSTRACT	18. NUMBER OF PAGES	19a. NAME OF RESPONSIBLE PERSON
a. REPORT	b. ABSTRACT	c. THIS PAGE			
unclassified	**unclassified**	**unclassified**	**UU**	**18**	

INTRODUCTION

The use of geodetic-type GNSS reception hardware and processing algorithms is growing for time and frequency transfer between atomic frequency standards over long distances. Reference **[1]** provided a very good review of geodetic time and frequency transfer. It is now recognized that: a) the pseudorange measurement errors, whether with white or colored noise and regardless of their source, are responsible for the solution-boundary discontinuities **[2]** and b) the analysis of these solution-boundary discontinuities gives an indication of the quality of individual station installations and may help in identifying corrective actions. Using best practices for the control of the environment of the GNSS reception hardware is no doubt the most effective method for eliminating most sources of errors on pseudoranges, e.g. multipath, near-field reflections, or temperature dependencies. However, for various reasons, cost being the principal one, these environment control methodologies cannot always be implemented in remote locations, or for large networks. Also, from an operational standpoint, unless the reception equipment itself simultaneously loses lock on all satellite signals, there is a compelling argument not to introduce discontinuities in processing over intervals where the hardware was able to maintain phase connection.

Since 2005, when **[1]** predicted the development of tools/software to remove the burden of complex geodetic computations for non-geodesists, many such tools have appeared from various groups in the community. Most of these tools take advantage of the International GNSS Service (IGS) satellite clock and orbit products **[3]** in single-station processing and all have two principal objectives in common: the removal or attenuation of discontinuities in the clock series that arise at solution time boundaries and, more recently, its corollary, the resolution of the integer nature of undifferenced carrier-phase ambiguities. To achieve this goal, the newly developed tools use a range of methods: processing over multiple days **[4]** and overlapping solutions **[5,6],** completely disregarding the pseudoranges in carrier-phase-only processing **[7]**, resolving single-differenced floating ambiguity estimates to integers **[8]**, or connecting the carrier-phase ambiguities between adjacent solutions **[9]**. Also, GNSS frequency transfer results are now combined with collocated independent time transfer techniques such as Two-Way Satellite Time and Frequency Transfer (TWSTFT) **[10,11]**.

The issue of pseudorange errors affecting clock estimates in GNSS processing prompted us to take a closer look at the fundamental observation parameterization used in the clock estimation process. In the subsequent sections, we will describe the new decoupled-clock observation model and the rationale that led to its development. We will then test it in a network-mode station and with a satellite clock estimation least-squares filter developed at NRCan for the computation of GPS wide-area corrections.

GPS OBSERVATION MODELING

The decoupled-clock observation model has been introduced in **[12,13]**. We will give a summary of the model and the supporting rationale.

COMMON-CLOCK MODEL

Dual-frequency GPS pseudorange and carrier-phase observations are expressed as follows:

$$
\begin{aligned}
P_1 &= \rho + T + \quad I + c\left(dt^r - dt^t\right) + b^r_{P1} - b^t_{P1} + \varepsilon_{P1} \\
P_2 &= \rho + T + q^2 I + c\left(dt^r - dt^t\right) + b^r_{P2} - b^t_{P2} + \varepsilon_{P2} \\
\lambda_1(\Phi_1 + N_1) = L_1 &= \rho + T - \quad I + c\left(dt^r - dt^t\right) + b^r_{L1} - b^t_{L1} + \varepsilon_{L1} \\
\lambda_2(\Phi_2 + N_2) = L_2 &= \rho + T - q^2 I + c\left(dt^r - dt^t\right) + b^r_{L2} - b^t_{L2} + \varepsilon_{L2}
\end{aligned}
\qquad \text{(Eq. 1)}
$$

where *P*i are pseudoranges and *L*i are carrier phases on each of the GPS base frequencies – here, for simplicity, we do not distinguish between CA-code or P-code pseudoranges (**[12]** provides important details on the different pseudorange types), ρ is the geometric propagation delay, T is the propagation delay through the troposphere, I the propagation delay on the L1 frequency due to the ionosphere, q^2 the conversion factor of ionospheric propagation delay for the L2 frequency, c the speed of light in vacuum, dt^r and dt^t respectively the receiver and transmitter clock offset with respect to a common hypothetical reference, and the ε parameters express measurement errors. The b_*^* parameters are receiver- and transmitter-specific bias parameters for each observable type. Dual-frequency processing algorithms eliminate the ionospheric propagation delay to the first order by respectively combining the pseudoranges and carrier phases on the L1 and L2 transmitted frequencies to generate the ionosphere-free observables:

$$
\begin{aligned}
P_3 &= \frac{77^2 P_1 - 60^2 P_2}{77^2 - 60^2} \\
&= \rho + T + c\left(dt^r - dt^t\right) + b^r_{P3} - b^t_{P3} \qquad + \varepsilon_{P3}
\end{aligned}
\qquad \text{(Eq. 2)}
$$

$$
\begin{aligned}
L_3 &= \frac{77^2 L_1 - 60^2 L_2}{77^2 - 60^2} \\
&= \rho + T + c\left(dt^r - dt^t\right) + b^r_{L3} - b^t_{L3} - \lambda_3 N_3 + \varepsilon_{L3}
\end{aligned}
\qquad \text{(Eq. 3)}
$$

where the receiver and transmitter clock parameters are the same for pseudorange and carrier phase. The observable biases are usually considered negligible or as constants over time absorbed in the clock offset parameters. Yet **[2]** has shown the pseudorange biases are not always negligible and more importantly not always constant. When not properly accounted for in the parameterization, estimation processes will distribute these time-varying biases into all estimated parameters, primarily to those most mathematically correlated: clocks and ambiguities. The direct effect is the solution-boundary (usually daily) discontinuities for batch processing, as those observed in the IGS clock products **[1]**, or divergence or frequency errors in continuous filtering processes. These effects also reduce the ability of undifferenced data processing algorithms to resolve integer ambiguities. The effect of the biases are shown in Figure 1, where three relative clock solutions between two IGS stations (YELL and AMC2) equipped with hydrogen masers (HM) are displayed: 1) a simple pseudo-range solution, 2) a continuous least-squares filter using the above common-clock parameterization (Eq. 2,3), and 3) the IGS Rapid (IGR) clock solution. The IGR solution-boundary discontinuities are present and their sizes correlate well with the amplitude of the long-term variations of the pseudorange solution. Clock estimates from the filter solution are continuous, but show frequency errors when compared to the IGR (positive vs. negative slopes and vice versa). Note that, since within one daily batch the IGR solutions are combinations of ambiguity fixed solutions, these should represent the clock as 'seen' by the carrier phases. We will hereafter label this parameterization and any results thereof "common-clock."

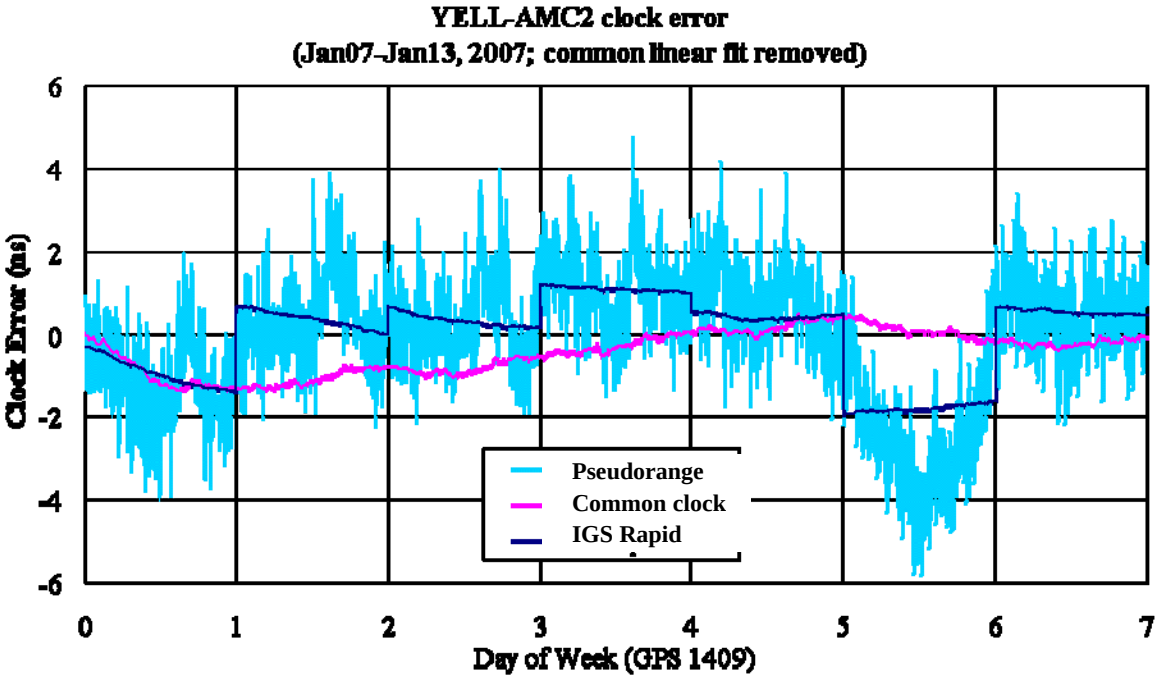

Figure 1. Three clock solutions for the YELL-AMC2 station pair involving two HM (from **[12]**).

DECOUPLED-CLOCK MODEL

Taking into account the biases in the parameterization leads to a new system of equations:

$$\begin{aligned} P_3 &= \rho(\vec{x}^r, \vec{x}^t) + \overline{zpd} \cdot map_T + c\left(\overline{dt^r_{L3}} - \overline{dt^t_{L3}}\right) + \overline{B^r_{P3}} - \overline{B^t_{P3}} + v_{P3} \\ L_3 &= \rho(\vec{x}^r, \vec{x}^t) + \overline{zpd} \cdot map_T + c\left(\overline{dt^r_{L3}} - \overline{dt^t_{L3}}\right) - \lambda_3 \overline{N_3} + v_{L3} \end{aligned} \qquad \text{(Eq. 4)}$$

where overbars now express estimated parameters, $\rho()$ is the distance between transmitter and receiver instantaneous positions $(\vec{x}^r, \vec{x}^t)$ accounting for earth displacements and including relativistic corrections, map_T is the function mapping the local receiver zenith tropopheric delay *zpd* to the slant delay *T*, dt^r_{L3} and dt^t_{L3} are the receiver and transmitter carrier-phase clock offsets, B^r_{P3} and B^t_{P3} are the receiver and transmitter pseudorange biases (or decoupled "pseudorange clock offsets"), $\lambda_3 N_3$ is the L_3 carrier-phase ambiguity multiplied by its wavelength, and v_{P3} and v_{L3} the pseudorange and carrier-phase observation residual errors. Because λ_3 is ~6mm, too small to allow efficient integer ambiguity resolution if at all possible, we add the Melbourne-Wübenna observation combination **[14,15]**:

$$\begin{aligned} A_4 = L_4 - P_6 &= (77L_1 - 60L_2)/17 - (77P_1 - 60P_2)/137 \\ &= \overline{B^r_{A4}} - \overline{B^t_{A4}} - \lambda_4 \overline{N_4} + v_{A4} \end{aligned} \qquad \text{(Eq. 5)}$$

composed of the wide-lane phase combination L_4 and the pseudorange narrow-lane combination P_6. The λ_4 wavelength of ~86 cm allows easier integer resolution for N_4 which in turn, through parameter substitution, gives a wavelength of ~10.7 cm for N_3, better suited for integer resolution techniques.

As it stands, the system of equations formed by Eqs. 4 and 5 is singular, the biases and clock terms being linearly dependent. By decoupling the pseudorange and carrier-phase clock terms, we effectively removed the datum provided by the pseudorange measurements which allowed ambiguity estimation in a common-clock parameterization. We resolve this rank deficiency by providing an arbitrary ambiguity datum and this will yield ambiguous carrier-phase clock estimates. To provide a set of minimum-constraint, solvable normal equations, one ambiguity per carrier-phase clock less one, must be fixed to an arbitrary value. Additionally, one set of carrier-phase clock, pseudorange bias, and wide-lane bias parameters must be fixed as the network datum. This is similar to network processing using the common-clock parameterization where one clock must be fixed. To maintain the continuity of all parameters, this minimum set of fixed ambiguities and parameters must be carried over time, as satellites rise and set over receiving stations. This requires ambiguity bookkeeping algorithms for on-the-fly selection of integer resolved ambiguities to replace datum ambiguities disappearing from the system.

The decoupled-clock parameterization can be exploited in both network mode, where all transmitter and receiver clocks are solved for (less one datum set as we have already seen), as well as in a single receiver Precise Point Positioning (PPP) mode **[16,17]**, as was shown in **[13]**. The requirement here is a decoupled-clock network solution for the transmitter constellation, e.g., carrier-phase clocks, pseudorange and wide-lane biases, and fixing a single ambiguity parameter to provide the ambiguity datum. It was also shown in **[13]** that ambiguity resolution techniques could effectively be applied to the decoupled-clock parameterization.

The decoupled-clock model was implemented in a sequential least-squares filter which was originally developed for the generation of GPS wide-area corrections **[18]**. The filter accepts observations either from real-time data streams or from flat files in the estimation of satellite and station clocks, local station troposphere delay, and carrier-phase ambiguities, to which we add the pseudorange and wide-lane biases when using the decoupled-clock model. Stations and satellites positions are held fixed and a comprehensive set of conventions and physical models are adopted and used. Since the least-squares filter is continuous, it does not have solution-boundary issues. Using the common-clock model, the effect of pseudorange measurement errors is that the ambiguities become so much constrained to slightly erroneous values through accumulation of weight over time, that the system starts diverging after about a month or more. We initially resolved the divergence issue by adding small process noise to the ambiguity parameters. This, however, is not entirely satisfactory, as the pseudorange errors contaminate the clock solutions through the floating ambiguities, as was shown in Figure 1 and will be seen later.

EXPERIMENTAL ASSESSMENT

For the assessment of the new observation model, the least-squares filter was used to process the following dataset. Station coordinates were held fixed to their IGS05 coordinates of epoch and satellites to the IGR orbits. The GPS P1 and P2 pseudorange observation pair was used in the ionosphere-free combination, consistent with the IGS clock product convention. Receivers producing only CA pseudoranges are corrected for the C1-P1 biases **[19]**. The IGS convention for satellite and station absolute antenna phase center offsets and azimuth-elevation variations definition was used as well **[20]**.

Two solutions were generated with our processing engine: 1) using the common-clock model with introduction of process noise in the ambiguities and 2) using the decoupled-clock model.

DATA SET

We selected a data set from the IGS archive of daily 30-second RINEX format **[21]** files to form a reception network of 29 stations distributed around the globe, spanning 35 days in early 2008, specifically from MJD 54499 to 54533 inclusive, to which we added 11 stations of interest for time and frequency transfer purposes. The selection criteria for these 11 stations were: 1) timing laboratories operating geodetic GNSS receivers, 2) stations using atomic frequency standards, and 3) stations presenting a good reception record for the target period. The selection criteria for the 29 other stations were simply to ensure continuous tracking of the satellite constellation. This is of utmost importance for maintaining the ambiguity datum over time. Table 1 provides the list of selected stations and their GNSS reception equipment as reported by the logs maintained at IGS. IGR clock products, aligned to the IGR timescale, were also collected for comparison.

PSEUDORANGE MEASUREMENT ERRORS

An example of clock results contaminated by pseudorange measurement errors is shown in Figure 2, where the ambiguous phase clock solution is compared to the common-clock model and IGR clocks for the YELL and PTBB station pair. Figure 3 shows the pseudorange and wide-lane biases estimated in the decoupled-clock model filter process for the same period and station pair. The pseudorange biases show large variations between MJD 54503 and 54510 and between MJD 54526 and 54531. The response of the continuous common-clock model processing is to follow-on average the pseudorange biases and that of the IGR product is larger day-boundary discontinuities. The carrier-phase clocks from the decoupled-clock model are continuous over carrier-phase-continuous periods and their frequency is similar to that of IGS within each day. Daily averages of the estimated pseudorange biases were computed as well as an average over carrier-phase-continuous periods (Figure 3). There is a strong correlation between the IGR product day-boundary discontinuities and those implied by the daily averages of pseudorange bias. The correlation is even more striking in Figure 4, where the carrier-phase clocks were differenced with IGR clocks and then with IGR clocks corrected for the jumps implied by the daily pseudorange bias averages. Correcting the IGR clocks day-boundary discontinuities using daily averages of the pseudorange biases as estimated by the decoupled-clock model brought the consistency of both solutions at the sub-nanosecond level. The carrier-phase clock from the decoupled-clock model is largely immune to the pseudorange bias variations, although there are still half-daily oscillations in the differences that can be attributed to the carrier-phase solution, as will be shown in the stability analysis.

Table 2 lists RMS differences of nine station pairs for the decoupled-model carrier-phase clocks and IGR clocks, both corrected and uncorrected for day-breaks as explained above. Overall, the consistency of the decoupled carrier-phase clocks, the pseudorange biases and IGR clocks is at the 200-ps RMS level, or better. One should notice that the YELL-PTBB results are an extreme case caused by local conditions prevalent at the YELL station and well documented in **[1]**.

For the other stations pairs, where the pseudorange errors do not have such significant signatures, the improvement in RMS differences by correcting IGR clocks for day-breaks is not as pronounced. The overall improvement is, on average, about 50%, even when excluding the two extreme cases (NRC1, YELL). This is a reflection of the internal consistency of the IGS day-boundary discontinuities and decoupled-clock model pseudorange bias estimates and gives us confidence the new parameterization is sound.

Table 1. IGS stations selected and equipment list from MJD 54499 to 54533 as reported at *http://igs.org.*

STATION	RECEIVER	ANTENNA	FREQUENCY STANDARD	NOTES
TIMING LABORATORIES				
AMC2	ASHTECH Z-XII3T	AOAD/M_T	H-MASER	
BRUS	ASHTECH Z-XII3T	ASH701945B_M	H-MASER CH1-75	
IENG	ASHTECH Z-XII3T	ASH701945C_M	H-MASER	
NRC1	AOA SNR-12 ACT	AOAD/M_T	H-MASER	
NRL1	ASHTECH Z-XII3T	ASH701945C_M	H-MASER	
PTBB	ASHTECH Z-XII3T	ASH700936E	CESIUM	SNOW RADOME
SPT0	JPS LEGACY	AOAD/M_T	H-MASER	OSOD RADOME
SYDN	JPS E_GGD	ASH701945C_M	CESIUM	
TWTF	ASHTECH Z-XII3T	ASH701945C_M	STEERED H-MASER	SCIS RADOME
USN3	ASHTECH Z-XII3T	AOAD/M_T	H-MASER	
WAB2	ASHTECH Z-XII3T	ASH700936F_C	H-MASER	SNOW RADOME
OTHER ATOMIC FS				
COCO	ASHTECH UZ-12	AOAD/M_T	RUBIDIUM	
DARW	ASHTECH UZ-12 LEICA GRX1200GGPRO	ASH700936D_M	RUBIDIUM	
DAV1	ASHTECH UZ-12	ASH701945G_M	RUBIDIUM	AUST RADOME
DRAO	AOA BENCHMARK ACT	AOAD/M_T	RUBIDIUM	
KOKB	ASHTECH UZ-12	ASH701945G_M	H-MASER	
KOUR	JPS LEGACY	ASH701946.3	CESIUM	
LPGS	AOA BENCHMARK ACT	AOAD/M_T	RUBIDIUM	
MAS1	ASHTECH Z-XII3	AOAD/M_T	CESIUM	
MIZU	SEPT POLARX2	TPSCR3_GGD	CESIUM	
OUS2	SEPT POLARX2	TPSCR3_GGD	RUBIDIUM	
SANT	ASHTECH UZ-12	AOAD/M_T	CESIUM	JPLA RADOME
SUTM	AOA BENCHMARK ACT	AOAD/M_T	RUBIDIUM	
TIDB	ASHTECH Z-XII3	AOAD/M_T	H-MASER	JPLA RADOME
TOW2	ASHTECH UZ-12	AOAD/M_T	RUBIDIUM	AUST RADOME
YELL	AOA SNR-12 ACT	AOAD/M_T	H-MASER	
OTHER STATIONS				
CHPI	ASHTECH UZ-12	ASH701945C_M	QUARTZ/INTERNAL	
FAA1	JPS LEGACY	ASH701945B_M	QUARTZ/INTERNAL	
HYDE	LEICA GRX1200GGPRO	LEIAT540GG	UNSPECIFIED	
ISPA	ASHTECH UZ-12	ASH701945E_M	QUARTZ/INTERNAL	SCIT RADOME
KARR	ASHTECH UZ-12	AOAD/M_T	QUARTZ/INTERNAL	AUST RADOME
MALI	JPS LEGACY	ASH701946.3	UNSPECIFIED	
MKEA	ASHTECH Z-XII3	AOAD/M_T	QUARTZ/INTERNAL	
OHI2	JPS E_GGD	AOAD/M_T	QUARTZ/INTERNAL	UNSPEC. RADOME
OHI3	TPS E_GGD	ASH701941.B	QUARTZ/INTERNAL	SNOW RADOME
RCMN	LEICA GRX1200GGPRO	LEIAT540GG	UNSPECIFIED	LEIS RADOME
SEY1	ASHTECH UZ-12	ASH701945B_M	QUARTZ/INTERNAL	UNSPEC. RADOME
TASH	UNSPECIFIED			
ULAB	AOA SNR-8000 ACT	AOAD/M_T	UNSPECIFIED	

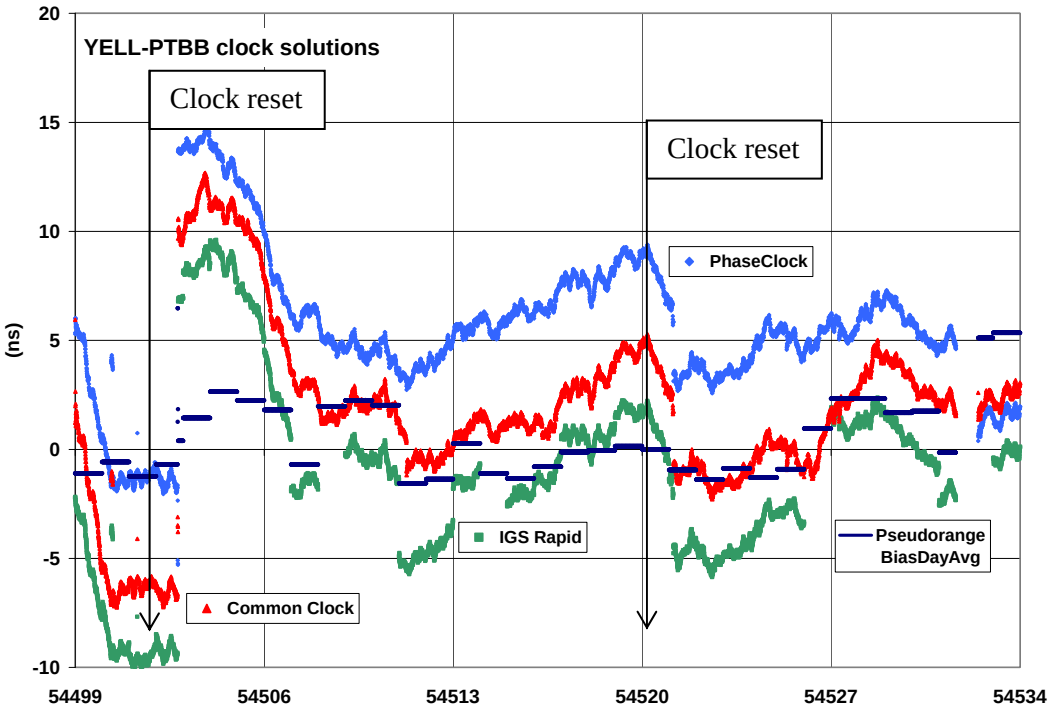

Figure 2. Thirty-five-day decoupled-clock solution for the YELL-PTBB station pair. Common-clock model and IGR solutions included for comparison. All solutions have a common frequency offset and drift removed and are arbitrarily offset in phase for display. Daily average of pseudorange biases included.

Table 2. RMS of differences between decoupled-clock model carrier-phase clocks and IGR corrected and uncorrected for day-breaks. The "Partial" row excludes pairs with NRC1 and YELL.

Station pair	# diff	PhaseClock-IGS RMS (ns)	PhaseClock – IGScorr. RMS (ns)	Improv. %
AMC2-PTBB	7591	0.142	0.111	22.0
BRUS-PTBB	9375	0.195	0.064	67.1
IENG-PTBB	9361	0.103	0.066	35.8
KOKB-PTBB	9377	0.237	0.135	43.1
NRC1-PTBB	9314	0.729	0.197	73.0
SPT0-PTBB	9294	0.209	0.111	46.7
TWTF-PTBB	9377	0.220	0.129	41.4
USN3-PTBB	8428	0.263	0.119	54.9
YELL-PTBB	8789	1.365	0.200	85.4
Partial	**72167**	**0.247**	**0.115**	**53.4**
Overall	**90270**	**0.534**	**0.136**	**74.5**

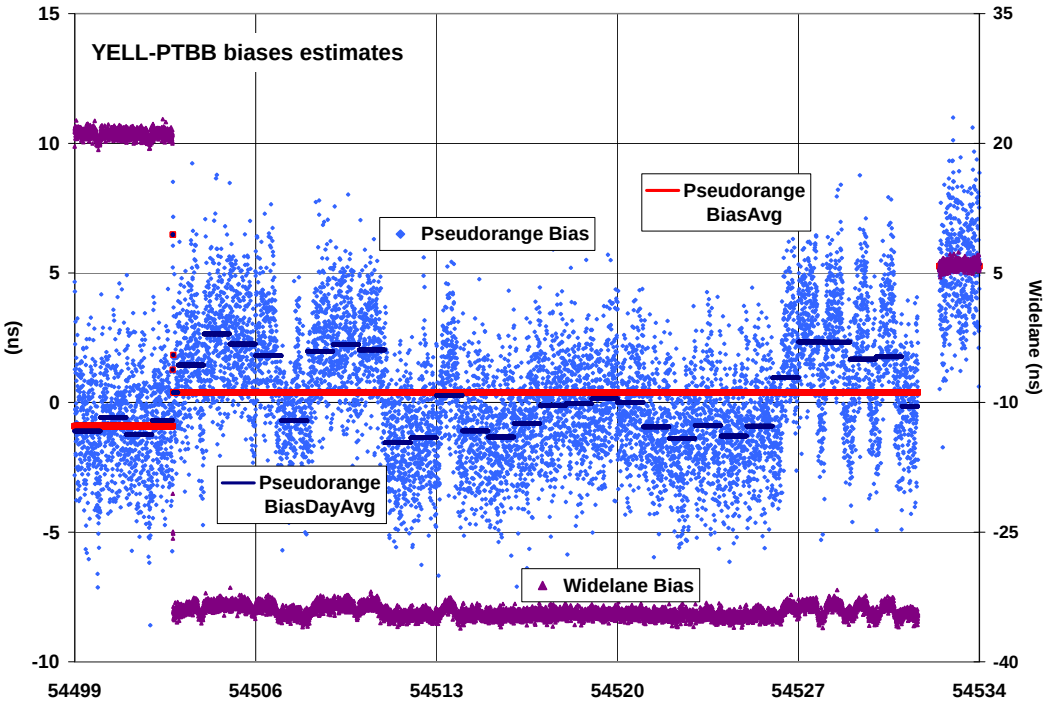

Figure 3. Pseudorange and wide-lane biases for the same period and station pair. Daily averages (black) of the estimated pseudorange biases as well as straight average (red) over the three phase-continuous periods are plotted.

The noise characteristics of the estimated pseudorange biases were further analyzed using Overlapping Allan deviations, as shown in Figure 5. The Overlapping Allan deviations show little differences in the short term and only small differences occur over the longer averaging intervals. Further analysis will be required to investigate their significance.

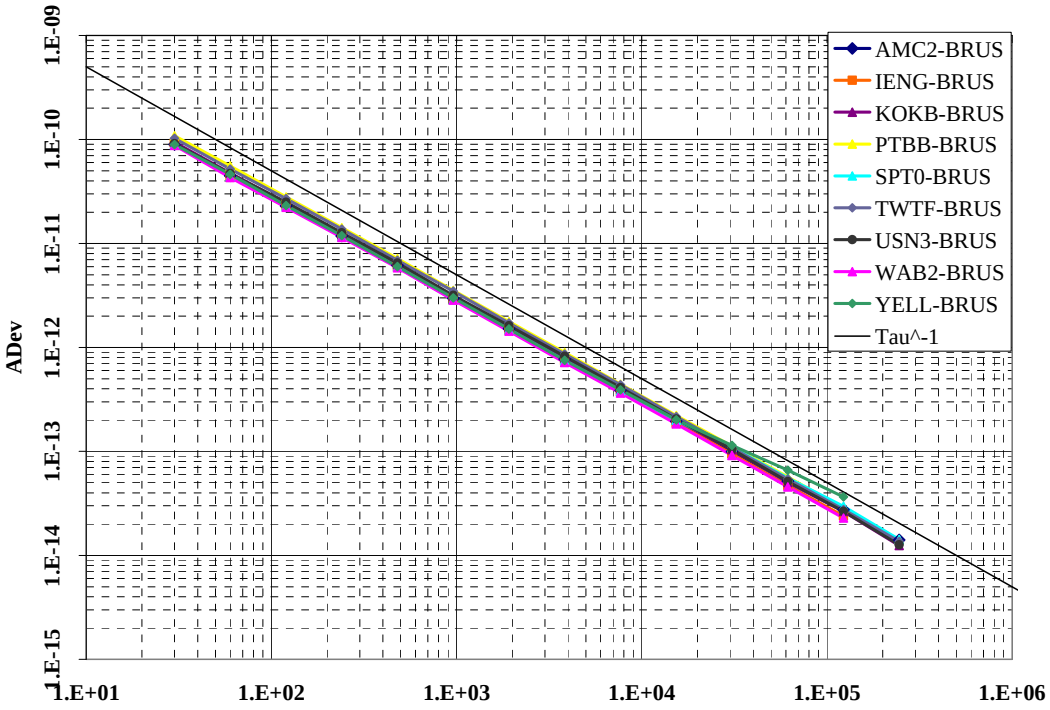

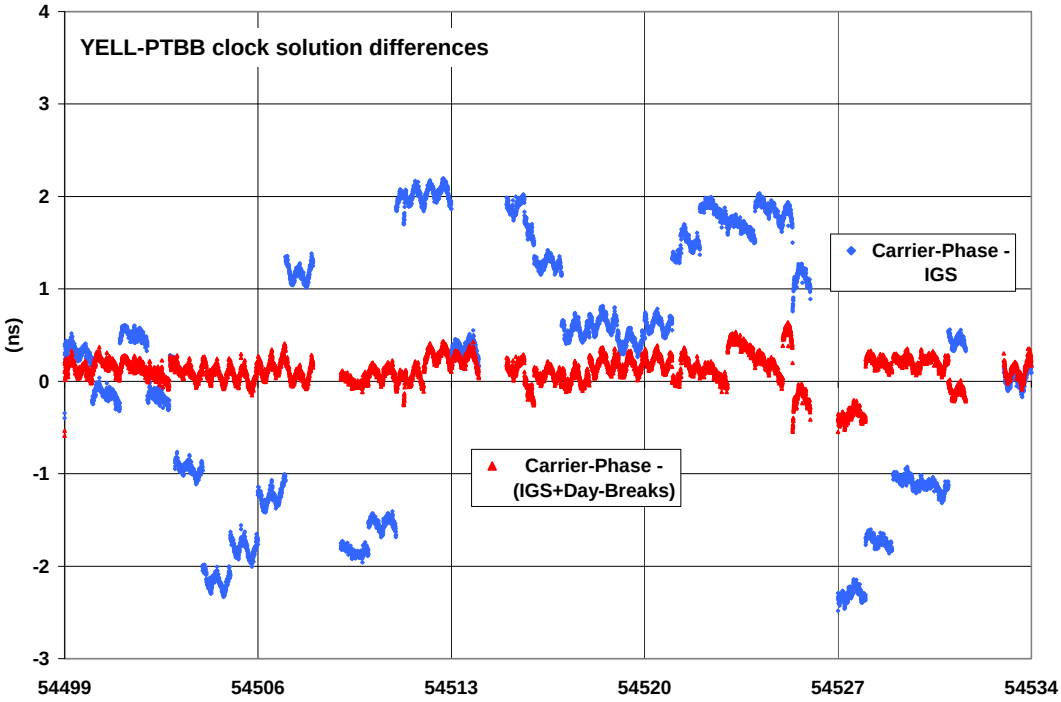

Figure 4. Differences between carrier-phase clock and IGR (blue) and IGR corrected for the day-breaks implied by the daily averages of pseudorange biases (red).

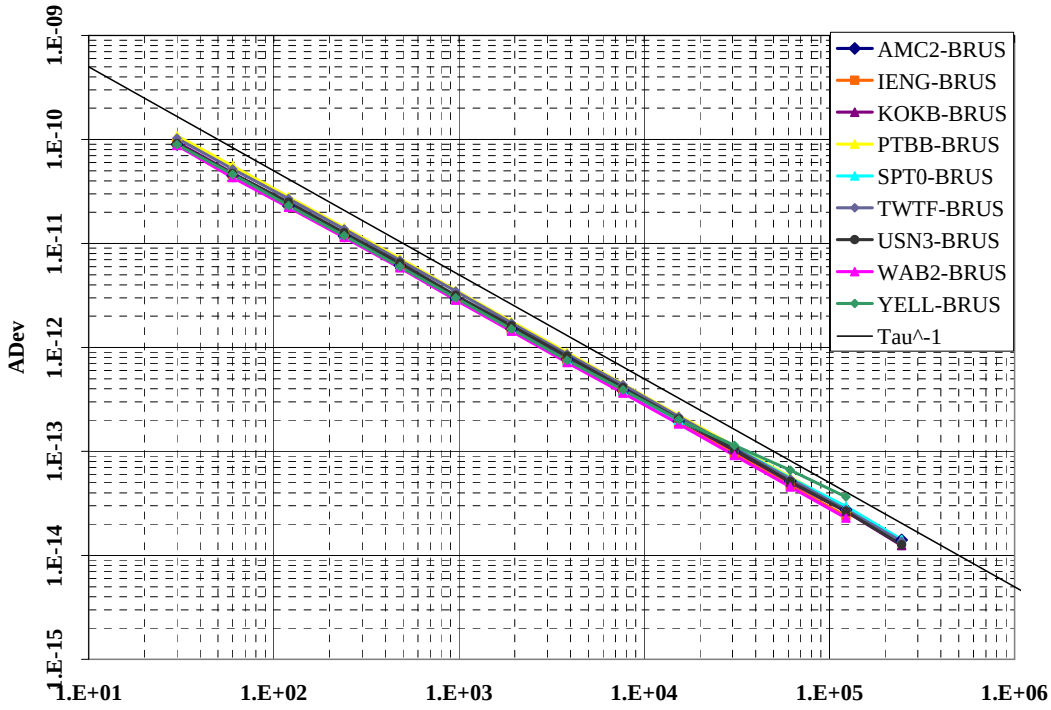

Figure 5. Overlapping Allan deviation of pseudorange bias estimates for all station pairs, datum jumps removed. Tau^{-1} noise line shown.

STABILITY ANALYSIS

We performed a stability analysis of the carrier-phase clock, computing their Overlapping Allan deviations. For each of the baselines listed in Table 3, we selected the stated periods within the 35 days where there were no clock resets, no ambiguity datum resets, and no missing days in the IGS clock solutions. Frequency series were generated from the following clock solutions: 1) the decoupled-clock model carrier-phase clock, 2) the carrier-phase clocks where we impose the day-breaks implied by the daily averages of estimated pseudorange biases, 3) the common clock solution, 4) the IGR clock solution, and 5) the IGR clock model, excluding those intervals crossing day-boundaries. The last case is not realistic and here considered an ideal case, i.e. IGS quality clocks without day-boundary discontinuities and, thus, uncontaminated by pseudorange errors. Data gaps with respect to the nominal solution intervals (300 seconds for the IGR and 30 seconds for the other series) were considered as missing data.

Table 3. Selected station pairs and associated periods for stability analysis.

Station pair	Period	#days
AMC2-BRUS	54517.69 – 54529.53	11.84
IENG-BRUS	54519.78 - 54529.53	9.74
KOKB-BRUS	54501.33 – 54515.77	14.44
PTBB-BRUS	54501.33 – 54529.53	12.66
SPT0-BRUS	54515.78 - 54529.53	13.75
TWTF-BRUS	54515.78 - 54529.53	13.75
USN3-BRUS	54515.78 - 54529.53	13.75
YELL-BRUS	54509.00 – 54515.77	6.77

Figure 6 shows the Overlapping Allan deviations for the YELL-BRUS and AMC2-BRUS station pairs. For the YELL-BRUS pair, affected most by YELL pseudorange biases, the improvement obtained by removing the day-boundary discontinuities from the IGR clocks is almost an order of magnitude. The carrier-phase clock stability, while not as good as the ideal case, is better than that obtained from the common clock model. Introducing day-breaks in the otherwise continuous carrier-phase clocks brings its stability to the level of the IGS solution. For the AMC2-BRUS pair, the common clock and decoupled-clock model solutions have similar stability, a little worse than the IGR. It appears the day-boundary discontinuities have little effect on that baseline. Worthy of notice is the small rise in the Allan deviations for the decoupled-clock model around a 6-hour interval. This confirms that the small half-day oscillations seen in Figure 4 come from the decoupled-clock model. This will be the subject of further analysis. Tables 4 and 5 respectively show the stability at 1-day and 1-hour for all the station pairs studied. For all station pairs, the carrier-phase clocks have improved long-term stability over the IGR and are close to the ideal case represented by IGR without day-boundaries. For most cases, it is as good or better than the common-clock results.

Table 4. Overlapping Allan deviation at 1 day for the frequency series and station pairs (units 10^{-15}).

Station pair	IGS without day-breaks	Carrier-phase clock	IGS with day-breaks	Carrier-phase with breaks	Common clock
AMC2-BRUS	2.5	2.5	2.8	2.8	2.5
IENG-BRUS	2.7	2.6	2.7	2.7	2.5
KOKB-BRUS	2.4	2.4	2.7	2.8	2.4
PTBB-BRUS	12.1	12.2	13.0	12.6	12.3
SPT0-BRUS	4.0	4.1	5.8	5.9	4.3
TWTF-BRUS	3.7	3.6	3.8	3.5	3.9
USN3-BRUS	2.3	2.3	2.2	2.2	1.9
YELL-BRUS	3.9	4.1	21.4	22.2	6.9

Table 5. Overlapping Allan deviation at 1 hour for the frequency series and station pairs (units 10^{-14}).

Station pair	IGS without day-breaks	Carrier-phase clock	IGS with day-breaks	Carrier-phase with breaks	Common clock
AMC2-BRUS	1.2	1.9	1.3	1.9	1.9
IENG-BRUS	1.4	1.4	1.5	1.5	1.9
KOKB-BRUS	1.3	2.5	1.6	2.6	2.1
PTBB-BRUS	5.6	5.8	5.8	5.8	5.8
SPT0-BRUS	1.3	1.2	1.8	1.8	1.4
TWTF-BRUS	1.2	2.0	1.5	2.0	2.0
USN3-BRUS	1.2	1.8	1.5	1.9	1.7
YELL-BRUS	1.0	1.6	8.7	9.0	3.4

CONCLUSION

The decoupled-clock model, a new parameterization of the GPS carrier-phase and pseudorange observations, and the rationale behind its development were described. The objective of the new parameterization is to remove the influence of pseudorange errors on the receiver clock estimates, which in batch solutions take the form of batch-boundary discontinuities which are too large to be accounted by noise characteristics of the atomic frequency standard to which the receiver is connected. The decoupled-clock model was implemented in a least-squares filter designed for network-mode station and satellite clock determinations for the generation of wide-area GPS corrections. Ambiguous carrier-phase clocks and pseudorange biases were obtained by processing 35 days of tracking data from a network of 39 globally distributed IGS stations, 11 of which are located at timing laboratories and several others are connected to atomic frequency standards. The same data set was processed using the common parameterization where pseudorange biases are not estimated and with process noise applied to the carrier-phase ambiguities estimation to prevent divergence.

Daily averages of the estimated pseudorange biases are consistent with the day-boundary discontinuities present in the IGR clock solutions. Using these averages to correct the IGR clock solutions brought their consistency with the continuous decoupled-clock model carrier-phase clock solutions at the sub-ns level even for the most affected stations YELL and NRC1. For the other stations where pseudorange contamination is not readily apparent, the clock solution consistency has improved by 50% over all the stations analyzed, giving us confidence in the new clock parameterization.

The stability of the carrier-phase clock solutions were analyzed in terms of Overlapping Allan deviations for the IGR clocks both with and without the intervals crossing the problematic day-boundaries, the later being an ideal case. For stations most contaminated by pseudorange biases, the improvement brought by the decoupled-clock model is significant, close to an order of magnitude in case of station YELL. For other stations, the improvement in stability is less significant.

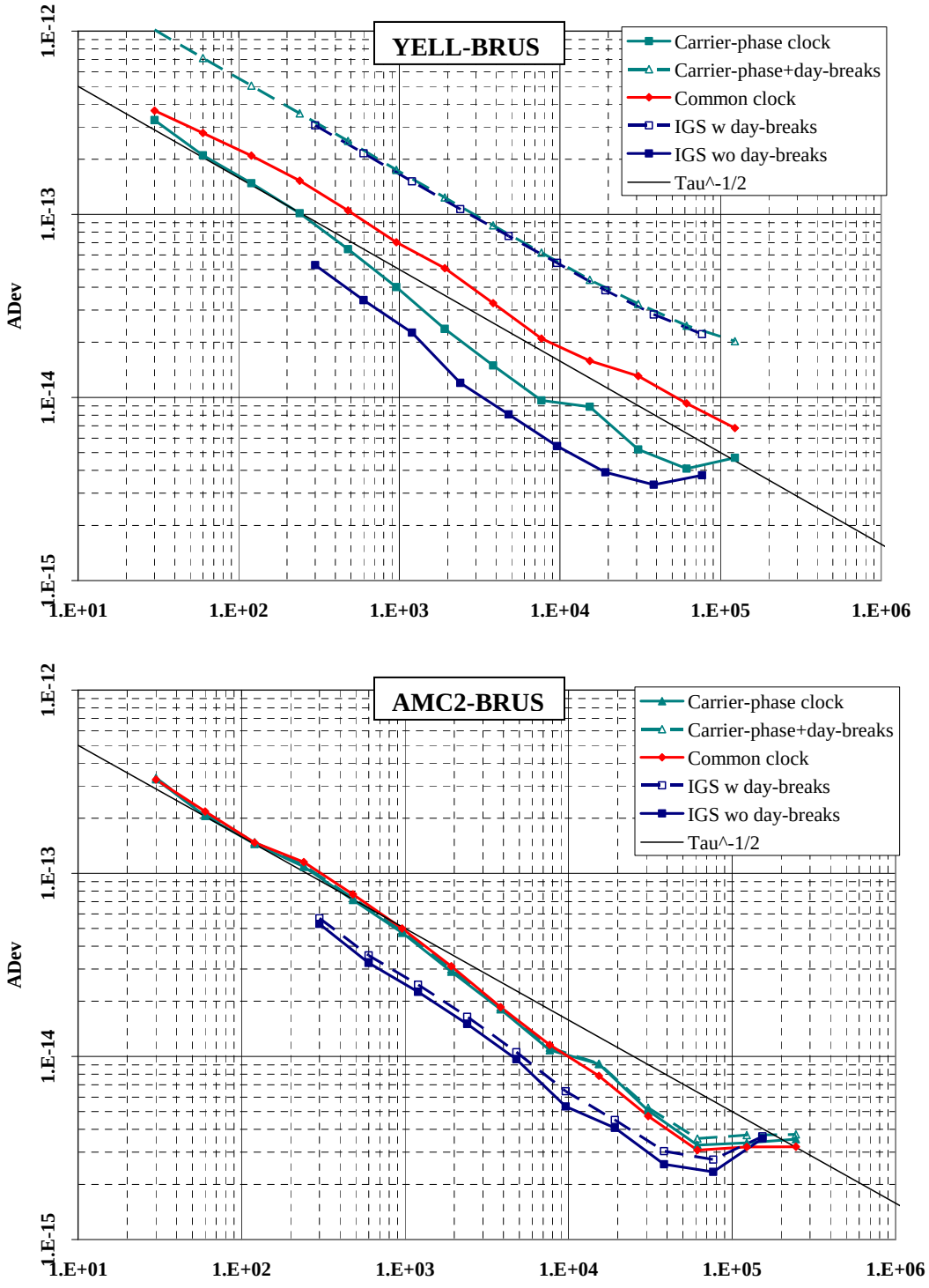

Figure 6. Overlapping Allan deviation for frequency series from YELL-BRUS and AMC2-BRUS station pairs. Tau$^{-1/2}$ noise line shown.

The objective of separating pseudorange errors within clock and ambiguity estimation is largely met by the decoupled-clock model, although for the most affected stations, there are still half-daily oscillations in the carrier-phase clocks that need further investigations. At its current stage of development, since the obtained clocks are ambiguous, the new clock parameterization yields frequency transfer accuracy that is consistent with the one implied by the IGR clocks without day-boundary discontinuities, for as long as both receivers maintain carrier-phase lock on the satellite constellation. The decoupled-clock ambiguity can be removed by combining with collocated independent time transfer methods, e.g. TWSTFT.

There is a side benefit that far exceeds just meeting the objective we have set. The new model explicitly reveals, on average, the noise structure of the pseudoranges, rather than seeing their effects compounded into the clock results as solution-boundary discontinuities. This opens areas of investigation and future development. Analysis of the noise properties on the pseudorange biases would allow the selection of the most effective function thereof to reintroduce the pseudorange datum in the results. For example, if the pseudorange biases for a particular station pair are white phase noise, simply adding their average over carrier-phase continuous periods to the carrier-phase clocks would allow connecting periods between carrier-phase losses of lock, thus extending the frequency transfer capability over very long continuous periods. Furthermore, if the ambiguity datum can be resolved to the correct integer, the carrier-phase ambiguity could be removed, yielding continuous carrier-phase quality GPS time transfer.

ACKNOWLEDGMENTS

The authors acknowledge all the institutions generously contributing their data to the IGS and especially the timing laboratories mentioned in this paper. Also acknowledged are the many institutions forming the IGS for the high-quality products. Finally, the contribution by Serena Zanetta from the Politecnico di Torino is hereby acknowledged. This paper is published under the NRCan Earth Science Sector (ESS) Contribution Number/Numéro de contribution du SST: 20080546.

REFERENCES

[1] J. Ray and K. Senior, 2005, "*Geodetic techniques for time and frequency comparisons using code and phase measurements,"* **Metrologia, 42,** 215-232.

[2] P. Defraigne and C. Bruyninx, 2007, "*On the link between GPS pseudorange noise and day-boundary discontinuities in geodetic time transfer solutions,*" **GPS Solutions, 11,** 239-249.

[3] J. M. Dow, R. E. Neilan, and G. Gendt, 2005, "*The International GPS Service (IGS): Celebrating the 10th Anniversary and Looking to the Next Decade,"* **Advances Space Research**, **36**, 320-326.

[4] D. Orgiazzi, P. Tavella, and F. Lahaye, 2005, "*Experimental assessment of the time transfer capability of Precise Point Positioning (PPP),*" in Proceedings of the Joint IEEE International Frequency Control Symposium (FCS) and Precise Time and Time Interval (PTTI) Systems and Applications Meeting, 29-31 August 2005, Vancouver, Canada (IEEE Publication 05CH37664), pp. 337-345.

[5] N. Guyennon, G. Cerretto, P. Tavella, and F. Lahaye, 2007, "*Further characterization of the time transfer capabilities of Precise Point Positioning (PPP),*" in Proceedings of TimeNav'07, IEEE Frequency Control Symposium (FCS) Joint with the 21st European Frequency and Time Forum (EFTF), 29 May -1 June 2007, Geneva, Switzerland (IEEE Publication 07CH37839), pp. 399-404.

[6] T. Gotoh, M. Fujieda, and J. Amagai, 2007, "*Comparison study of GPS carrier phase and Two-way Satellite Time and Frequency Transfer,*" in Proceedings of TimeNav'07, IEEE Frequency Control Symposium (FCS) Joint with the 21st European Frequency and Time Forum (EFTF), 29 May-1 June 2007, Geneva, Switzerland (IEEE Publication 07CH37839), pp. 1188-1193.

[7] P. Defraigne, C. Bruyninx, and N. Guyennon, 2007, "*PPP and phase-only GPS time and frequency transfer,*" in Proceedings of TimeNav'07, IEEE Frequency Control Symposium (FCS) Joint with the 21st European Frequency and Time Forum (EFTF), 29 May-1 June 2007, Geneva, Switzerland (IEEE Publication 07CH37839), pp. 904-908.

[8] J. Delporte, F. Mercier, D. Laurichesse, and O. Galy, 2007, "*Fixing integer ambiguities for GPS carrier phase time transfer,*" in Proceedings of TimeNav'07, IEEE Frequency Control Symposium (FCS) Joint with the 21st European Frequency and Time Forum (EFTF), 29 May-1 June 2007, Geneva, Switzerland (IEEE Publication 07CH37839), pp. 927-932.

[9] R. Dach, U. Hugentobler, T. Schildknecht, L.-G. Bernier, and G. Dudle, 2005, "*Precise continuous time and frequency transfer using GPS carrier phase,*" in Proceedings of the Joint IEEE International Frequency Control Symposium (FCS) and Precise Time and Time Interval (PTTI) Systems and Applications Meeting, 29-31 August 2005, Vancouver, Canada (IEEE Publication 05CH37664), pp. 329-336.

[10] Z. Jiang, G. Petit, and P. Defraigne, 2007, "C*ombination of GPS carrier phase data with a calibrated time transfer link.,*" in Proceedings of TimeNav'07, IEEE Frequency Control Symposium (FCS) Joint with the 21st European Frequency and Time Forum (EFTF), 29 May-1 June 2007, Geneva, Switzerland (IEEE Publication 07CH37839), pp. 1182-1187.

[11] Z. Jiang and G. Petit, 2008, "*Combination of GPS PPP and two-way time transfer for TAI computation,*" in Proceedings of the 39th Annual Precise Time and Time Interval (PTTI) Applications and Systems Meeting, 26-29 November 2007, Long Beach, California, USA (U.S. Naval Observatory, Washington, D.C.), pp. 195-202.

[12] P. Collins, 2008, "*Isolating and estimating undifferenced GPS integer ambiguities,*" in Proceedings of ION National Technical Meeting, 28-30 January, 2008, San Diego, California, USA (Institute of Navigation, Alexandria, Virginia), pp. 720-732.

[13] P. Collins, F. Lahaye, P. Héroux, and S. Bisnath, 2008, "*Precise Point Positioning with ambiguity resolution using the decoupled clock model,*" in Proceedings of the 21st International ION GNSS Meeting, 16-19 September 2008, Savannah, Georgia, USA (Institute of Navigation, Alexandria, Virginia), in press.

[14] W. G. Melbourne, 1985, "*The case for ranging in GPS-based geodetic systems,"* in Proceedings of the First International Symposium on Precise Positioning with the Global Positioning System, U.S. Department of Commerce, 15-19 April 1985, Rockville, Maryland, USA, **Vol. 1**, pp. 373-386.

[15] G. Wübenna, 1985, "*Software developments for geodetic positioning with GPS using TI-4100 code and carrier measurements,*" in Proceedings of the First International Symposium on Precise Positioning with the Global Positioning System, U.S. Department of Commerce, 15-19 April 1985, Rockville, Maryland, USA, **Vol. 1**, pp. 403-412.

[16] J. F. Zumberge, M. B. Heflin, D. C. Jefferson, M. M. Watkins, and F. H. Webb, 1997, "*Precise point positioning for the efficient and robust analysis of GPS data from large networks*," **Journal of Geophysical Research**, **102**, 5005-5018.

[17] P. Héroux and J. Kouba, 2001, "*GPS Precise Point Positioning using IGS orbit products*," **Physics and Chemistry of the Earth (A)**, **26**, 572-578.

[18] F. Lahaye, P. Collins, P. Héroux, M. Daniels, and J. Popelar, 2001, "*Using the Canadian Active Control System (CACS) for Real-Time Monitoring of GPS Receiver External Frequency Standards,"* in Proceedings of the 14th International ION GPS Meeting, 11-14 September 2001, Salt Lake City, Utah, USA (Institute of Navigation, Alexandria, Virginia), pp. 2220-2228.

[19] P. Collins, Y. Gao, F. Lahaye, P. Héroux, K. MacLeod, and K. Chen, "*Accessing and Processing Real-Time GPS Corrections for Precise Point Positioning − Some User Considerations,"* in Proceedings of the 18th International ION GNSS Meeting, 13-16 September 2005, Long Beach, California, USA (Institute of Navigation, Alexandria, Virginia), pp. 1483-1491.

[20] *ftp://igscb.jpl.nasa.gov/pub/station/general/igs05.atx*

[21] *http://igscb.jpl.nasa.gov/igscb/data/format/rinex211.txt*